Open Ceramics 14 (2023) 100356

Contents lists available at ScienceDirect

Open Ceramics

journal homepage: www.sciencedirect.com/journal/open-ceramics

The effects of mixing non-metal atoms in the B1 structured transition metal carbo-nitrides on their structure and mechanical properties: $HfC_{1-x}N_x$

Brennan R. Watkins [a,*], Jessica J. Lopez [b], Xiao-Xiang Yu [b], Gregory B. Thompson [b], Christopher R. Weinberger [a,c]

[a] Department of Mechanical Engineering, Colorado State University, Fort Collins, CO, 80523, USA
[b] Department of Mechanical and Metallurgical Engineering, University of Alabama, Tuscaloosa, AL, 35487, USA
[c] School of Advanced Materials Discovery, Colorado State University, Fort Collins, CO, 80523, USA

ARTICLE INFO

Handling Editor: Dr P Colombo

Keywords:
Ultrahigh temperature ceramics
Carbides
Nitrides
Modeling
Theory
Mechanical properties

ABSTRACT

In this paper, we utilize density functional theory to explore how alloying the carbide and nitride of a group IVB transition metal affects the phase stability and mechanical properties; we place an emphasis on elastic and dislocation properties, taking the HfC-HfN system as an example. An evolutionary algorithm is used to identify the ordered carbonitrides and the enthalpies of formation are compared with special quasi-random structures to identify this system's tendency to order and form a solid solution. The variation of elastic constants with composition is examined, and the computed elastic constants are used to predict the theoretical hardness. The GSF curves for various compositions are computed to determine how alloying would affect dislocation behavior. These results show that while there may be a modest peak in elastic response, the resistance to dislocation motion does not particularly show a peak. Furthermore, the alloying of HfC with HfN reduces the resistance to slip almost universally, and helps stabilize dislocations on {111} planes through the stabilization of an intrinsic stacking fault. These results are compared to previous in-depth analysis of the HfC-TaC system, allowing for comparisons between metal and non-metal alloying strategies.

1. Introduction

Transition metal carbides (TMCs) and transition metal nitrides (TMNs) belong to a class of ultra-high-temperature ceramic materials, and are often studied for their extremely high melting temperatures and good low-temperature hardness [1–3]. These properties make TMCs and TMNs well-suited for wear-resistant hard coatings as well as heat-shielding materials for aerospace applications [1,4–7]. Due to the complex mixture of covalent, metallic, and ionic bonding within these materials, many properties are highly composition-dependent; this has led to significant interest in creating solid solutions or alloys of these materials. For example, while HfC and TaC are reported to have the highest melting temperatures of any binary compounds, some reports have shown that $Ta_{0.8}Hf_{0.2}C$ has an even higher melting temperature [8–10] and the lowest vaporization rate [11]. More recently, Hong and de Walle [12] predicted that some hafnium carbonitrides have melting temperatures significantly (~200 K) higher than the highest seen in the Hf-Ta-C system.

There is also significant interest in using mixing or alloying to improve the mechanical properties of these materials, with a particular emphasis on increasing hardness [13]. Holleck showed that the hardness peaked in rocksalt (B1) structured TMC/Ns near compounds that have valence electron concentrations (VEC) of 8.3–8.6 electrons per formula unit, suggesting that this represented some optimal bonding state. Following this work, a theoretical study by Balasubramanian et al. predicted a maximum value in both hardness and elastic stiffness for an HfC-HfN alloy with a VEC of approximately 8.25 electrons per formula unit (f.u.) [14]. Other *ab-initio* research into carbide-nitride mixing, performed by Jhi et al., predicted bulk moduli for TiC–TiN mixtures that were greater than the expected linear interpolation between the bulk moduli of the binary compound s [15]. Furthermore, Yang et al. demonstrated that there may be a maximum hardness—both for microindentation and nanoindentation—in the HfC-HfN system at an intermediate composition [16]. Buinevich et al. also experimentally concluded that a hafnium carbonitride mixture had a higher melting temperature and possibly higher hardness than the binary compound

* Corresponding author.
E-mail address: brenno@colostate.edu (B.R. Watkins).

https://doi.org/10.1016/j.oceram.2023.100356
Received 31 December 2022; Received in revised form 1 March 2023; Accepted 3 April 2023
Available online 6 April 2023

HfC, though no comparison with HfN was made [17]. These ideas of tailoring hardness through mixing, and specifically VEC optimization, has been revived with the development of high entropy ceramics, wherein the mixing of many elements has been used to change mechanical properties [18–22]. While the development of high entropy carbides and nitrides has the potential to increase the design space of TMCs/TMNs, this new design space emphasizes the question of how the different chemical species affect mechanical properties—collectively as well as individually—creating further need for fundamental studies of alloying and mechanical properties in the TMCs/TMNs.

While there are theoretical studies [14,23–25] of how composition affects mechanical properties, they often do not investigate the fundamental carriers of plastic deformation: dislocations. The notable exception is the work by Smith et al. [26], who specifically examined how the mixing would affect elastic constants, hardness, and the slip plane choice of dislocations in mixed TaC-HfC compounds. They found that as the composition varies from HfC to TaC, there is a peak in the computed theoretical hardness at about $Hf_{0.75}Ta_{0.25C}$ and that a metastable intrinsic stacking-fault (ISF) forms on the {111} plane at a similar composition. This can be interpreted to occur at a VEC of 8.25 electrons/f.u., which is within the range of postulated optimal VEC in these materials [13,14,27].

The goal of this work is to examine how mixing the non-metal species, e.g. carbon and nitrogen, affects similar properties of these materials. If the VEC is the most important predictor, we should see similar trends between the HfC-TaC system and the HfC-HfN system and thus pick the HfC-HfN system for this detailed study. Previous experimental investigations into the plastic deformation in HfC and HfN relatively limited, but prior work has demonstrated that HfC primarily cracks under indents with limited dislocation slip associated with the ⟨110⟩{110} slip system [28]. On the other hand, HfN (under four-point bending at room temperature) slips via the ⟨110⟩{111} system [29]. The differences in the dislocations and amount of plasticity has been attributed to the presence of an ISF in the group IVB nitrides and group VB carbides (e.g. HfN and TaC), and its absence in the group IVB carbides (e.g. HfC) [28–30]. Thus, the existence of the ISF in these materials is thought to be very important in regulating slip [30] and it is critical to how the ISF energy varies as the ratio of non-metal species is varied from pure HfC (with no ISF) to pure HfN (with an ISF).

Thus, in this work we will directly compare the enthalpies of formation, ordering-disordering energetics, elastic constant trends, theoretically predicted hardness, stacking fault energies and dislocation property trends as a function of composition and valence electron concentration in the HfC-HfN system. We then compare the theoretically predicted hardness to experimental measurements to ascertain the relative accuracy of the computational predictions. This will address an important fundamental question regarding how similar are metal- and nonmetal-atom mixing (via substitution on the metal and nonmetal rocksalt sublattices) in the *B*1-structured transition metal carbides.

2. Materials and methods

2.1. Computational methodology

We predicted the stoichiometric compounds and their crystal structures using the evolutionary algorithm implemented in the USPEX code [31–33]; this approach features global optimization with real-space representation and flexible physically motivated variation operators. For each candidate structure generated by USPEX, we performed density-functional theory (DFT) simulations using the Vienna *Ab-Initio* Simulation Package (VASP) [34–36]. The details of the VASP simulations, including reciprocal space integration, pseudopotentials, and exchange correlations can be found in the description of the DFT parameters below. The evolutionary algorithm is based on generations where the first generation consists of 50 randomly-generated structures, with unit cells containing up to 30 atoms. Each subsequent generation contained 40 structures; these were produced via the following mechanisms: 40% by heredity, 20% by soft mutation, 20% by transmutation, and 20% by random generation. During heredity, selected section planes of multiple 'parent' structures are combined to produce a new structure; soft mutation involves swapping the positions of unlike atoms (C and N, in this case), and transmutation involves the application of a strain to the lattice vectors. These structures were produced from 70% of the lowest-energy structures of the previous generation, the other 30% being discarded. We determined the thermodynamically stable structures using a convex-hull construction, wherein a structure is deemed stable if its enthalpy of decomposition into any other compound is positive. We continued these calculations until the stable structures remained unchanged for 10 generations. This method has proven successful in the study of the transition metal carbides for determining vacancy and metal atom ordering in previous studies [26,37–41]. Further details about the algorithm can be found in Refs. [31,32,42]. In addition to these ordered phases, we modeled 'disordered' phases using special quasi-random structures (SQSs) generated via the Alloy Theoretic Automated Toolkit (ATAT) [43]. Our SQSs were based on a 2 × 2× 2 conventional cell of the rocksalt (*B*1) structure, and thus contained 64 atoms. This choice of simulation cell shape and size allowed us to estimate both the formation enthalpy and the elastic stiffnesses of each quasi-random phase, more details can be found in the Supplemental Material.

For the DFT calculations in VASP, we used the projector augmented wave (PAW) method [44] in conjunction with the generalized-gradient approximation (GGA), parameterized by Perdew, Burke and Ernzerhof (PBE) [45]. In the case of Hf, we selected the 4-electron ($6s^25d^2$) pseudopotential; for C and N, we used the 4-electron ($2s^22p^2$) and 5-electron ($2s^22p^3$) pseudopotentials, respectively. For the elastic constants and formation enthalpies, the plane-wave cutoff energy was set to 600 eV and an automatically-generated K-point mesh with a resolution of $2\bullet\pi\bullet0.0182$ Å^{-1} was used to integrate the reciprocal space [46]. For the GSF energy curves, a vacuum gap of 15 Å was created normal to the shear plane in order to prevent the stacking-fault from having a non-negligible interaction energy with its periodically-reproduced multiples above and below the simulation cell. Additionally, the reciprocal space was integrated with an automatically-generated $N \times N \times 1$ mesh (where N is an integer chosen for the appropriate K-point spacing, depending on the cell size) to further limit the effect of defect interactions away from the shear plane. All structural relaxations were considered fully converged when the change in total energy between two ionic relaxation steps was less than 1×10^{-5} eV.

2.2. Experimental details

Using HfC and HfN powders, we prepared ceramic billets with nominal compositions of HfC, 75HfC:25HfN (Hf_4C_3N), 25HfC:75HfN (Hf_4CN_3), and HfN. For the hafnium carbonitride compositions, we mixed the starting powders at the nominal C/N ratio by rotatory blending; the blending was performed for 4 h to achieve a homogeneous mixture prior to consolidation. We encapsulated all powders into Ta cans, which were hermetically sealed by tungsten inert gas (TIG) welding inside a glove box. The cans were then hot isostatically pressed (HIP) at a temperature of 2200 K and a pressure of 2×10^5 Pa for 1 h in a graphite filament furnace within an argon atmosphere.

After consolidation, the samples were cut and mounted into bake-lite polishing pucks whereupon they were metallographically polished to 1200 grit SiC paper followed a Vibromet® polish for 24 h in an aqueous 0.05 μm silica slurry until a mirror finish was achieved. The samples where then imaged in a Thermo Fisher Apreo S Scanning Electron Microscope (SEM) at 20 keV where the image contrast from the pores and consolidated grains was analyzed using the Image J® freeware platform. The computed porosity, Table 1, was calculated based on the area fraction of pores to the total image size. All samples achieved near full density.

Table 1
Porosity measurements extracted from area fraction measurements.

	Relative Density (%)	95% Confidence Interval
$Hf_4C_2N_1$	99.98	0.04
$Hf_4C_1N_2$	99.07	0.3
HfC	99.33	0.05
HfN	99.75	0.12

Fig. 1 is a representative SEM X-ray Energy Dispersive Spectroscopy of Hf_4C_2N sample taken at 20 keV accelerating voltage, confirming the compositional uniformity of the samples where the indents were taken. A more detailed microstructure characterization study of these samples was previously reported in Ref. [47]. In the present work, we have now collected hardness values from these samples using an array of 10 × 10 indents separated by 50 μm in a G200 KLA Agilent nanoindenter with a Berkovich diamond tip. These indentations were performed at a strain rate of 0.05 s^{-1}, to a final indentation depth of 1500 nm. The analysis of the hardness followed the Oliver and Pharr method [48] with the hardness values tabulated in Table 2.

3. Results and discussion

3.1. Phase stability & formation enthalpy

The computed enthalpies of formation for mixed hafnium carbo-nitrides, $HfC_{1-x}N_x$, can be seen in Fig. 2(a) with the reported stable crystal structures listed in Table S2. These values are plotted with respect to the composition coordinate $x = N/(C + N)$, or the number fraction of N atoms on the nonmetal sublattice. All of the structures shown are based on the B1 structure, as expected, with the crystal structures being defined by the ordering of the carbon and nitrogen atoms on the non-metal sublattice. These crystal structures are shown illustrated in Fig. 3. We also computed formation enthalpies for the 64-atom SQSs [49], which can be considered to have a disordered nonmetal sublattice. Unsurprisingly, the convex hull consists entirely of ordered phases and the formation enthalpies for the ordered structures are larger in magnitude (more negative) than those of the SQS hafnium carbonitrides by about 0.01 eV/atom. This ordering effect is comparable to that seen in the pseudo-binary HfC-TaC system investigated by Smith et al. [26], so the HfC-HfN system exhibits a similarly weak tendency to order. The low thermodynamic driving force for ordering indicates that long annealing times would be required to produce significant long-range ordering; thus, we expect nonmetal-atom ordering to be difficult, meaning that most synthesized hafnium carbo-nitrides would be random solid solutions. Accordingly, the remainder of our investigation into mechanical properties is done under the assumption of negligible long range ordering effects.

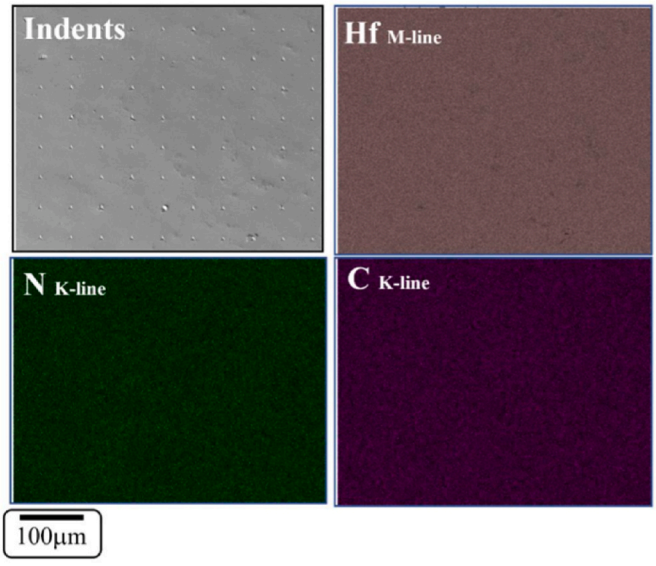

Fig. 1. Representative SEM image of an indent array and XEDS chemical maps for the Hf_4C_2N sample.

Table 2
The experimental hardness measurements in HfC, HfN, and the two hafnium carbonitrides.

Sample	HfC	$HfC_{0.67}N_{0.33}$	$HfC_{0.33}N_{0.67}$	HfN
Hardness (GPa)	32.2 ± 1.4	33.5 ± 4.2	31.8 ± 4.7	26.6 ± 1.5

The HfC-HfN solution appears to be a regular solution with a small negative enthalpy of formation. This is a common feature in of solutions of the pseudo-binary transition metal carbides [50–52]. The maximum difference in lattice constants is about 0.12 Å, which according to Tang et al. [51] would indicate either a very small positive or negative enthalpy of formation, as observed in our simulations. The as-computed lattice constants of HfN and HfC, as well as several intermediate-composition SQSs, are shown in Fig. 2(b); the variation in lattice constant is essentially linear with respect to composition, indicating an adherence to Vegard's law [53]. This further corroborates a high solubility of the two pseudo-binary solutions.

3.2. Elastic constants

The most frequently studied mechanical property of TMC/Ns theoretically is the elastic stiffness of the material due to its ease of calculation and the ability to estimate hardness from stiffness variations. Thus, we computed the elastic constants for both the ordered and disordered structures, in VASP; the results of which can be seen in Table 3 and Table S3. As previously reported by Jhi et al. [25], the cubic shear modulus C_{44} has a maximum at a composition of $x = 0.25$ (i.e. $HfC_{0.75}N_{0.25}$) which is illustrated in Fig. 4(a). However, this modulus alone is not representative of the material's resistance to elastic deformation during a hardness test; instead, it is reasonable to compute the average value of the shear modulus for a polycrystalline aggregate. Accordingly, over our range of C/N ratios, we computed the Hill average shear modulus [25]:

$$G \equiv \frac{1}{2}(G_V + G_R)$$

where G_V and G_R are the Voigt and Reuss shear moduli [54], respectively given by

$$G_V = \frac{1}{5}(C_{11} - C_{12} + 3C_{44})$$

$$G_R = 5\frac{C_{44}(C_{11} - C_{12})}{[4C_{44} + 3(C_{11} - C_{12})]}$$

for a crystal with cubic symmetry. Fig. 4(b) shows the Voigt, Reuss and Hill shear moduli for various compositions. Like the C_{44} modulus, these averaged shear moduli exhibit maxima at an intermediate composition; however, unlike C_{44}, the shear moduli suggest that a $HfC_{1-x}N_x$ polycrystal will have a maximum resistance to elastic shear deformation at a VEC of approximately 8.4 electrons per formula unit. While this does confirm the observations of Jhi et al. regarding this maximum, it is unclear if this is really important in terms of tailoring material properties. These elastic constant variations amount from our calculations to less than a 10% increase in stiffness. Thus, while there exists a peak in elastic stiffness, it is doubtful that this type of compositional engineering will produce superior stiff or hard materials.

Furthermore, to examine how these elastic constant variations would result in hardness variation, from previous theoretical predictions, as

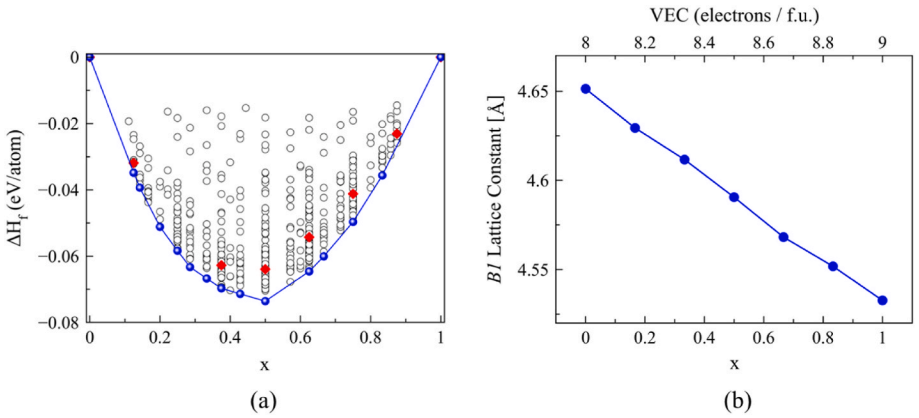

Fig. 2. (a) The enthalpy of formation of various $HfC_{1-x}N_x$ compounds as a function of composition x (or, equivalently, VEC). The most stable phases, represented with filled blue circle markers, are shown on the convex hull; less stable phases are shown as open circles. The SQS phases, shown as red diamonds, are unsurprisingly less stable than the ordered phases on the convex hull. (b) The as-computed lattice constants for the 64-atom $HfC_{1-x}N_x$ SQSs as a function of composition x, exhibiting a roughly linear trend. (For interpretation of the references to colour in this figure legend, the reader is referred to the Web version of this article.)

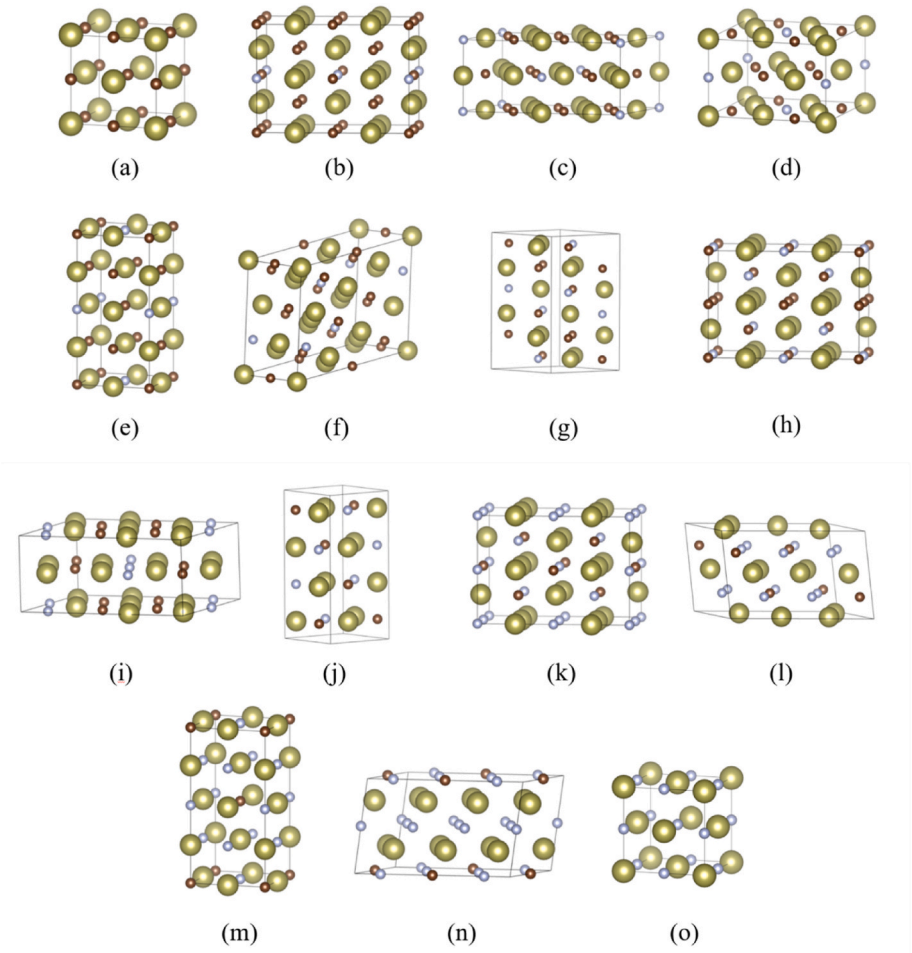

Fig. 3. Visualization of stable $HfC_{1-x}N_x$ phases found on the convex hull. In order of increasing HfN concentration, we have (a)$Fm\bar{3}m$ HfC, (b) Cmmm Hf_8C_7N, (c) C2/m Hf_7C_6N, (d) I4/m Hf_5C_4N, (e) I4/mmm Hf_4C_3N, (f) C2/m $Hf_7C_5N_2$, (g) C2/c Hf_3C_2N, (h) C222 $Hf_8C_5N_3$, (i) C2/m $Hf_7C_4N_3$, (j) I41/amd Hf_2CN, (k) C222 $Hf_8C_3N_5$, (l) C2/c $Hf_6C_2N_4$, (m) I4/mmm Hf_4CN_3, (n) C2/m Hf_6CN_5, and (o) $Fm\bar{3}m$ HfN.

well as compare with experiments we computed theoretical hardness values using the method developed by Chen et al. [55]:

$$H_V = 2\left(k^2 G\right)^{0.585} - 3$$

where B is the bulk modulus, given by

$$B = \frac{1}{3}(C_{11} + 2C_{12})$$

and k is Pugh's modulus, equal to the ratio G/B.

Fig. 5 shows the theoretical hardness predicted by this model as a function of C/N ratio and VEC. For comparison, we also plotted our experimentally-determined hardness, from Table 2, for the four hafnium carbonitride compounds, the experimental data of Holleck [13] and Yang et al. [16]. The theoretical hardness trends match the trends of the shear modulus showing a maximum near $x = 0.4$ or a VEC of 8.4. Collectively, the experimental results show similar trends to the model

Table 3
Computed and derived parameters for various hafnium carbonitrides. These quantities may serve as indicators of slip plane preference in these materials.

	HfC	$Hf_6C_5N_1$	$Hf_6C_4N_2$	$Hf_6C_3N_3$	$Hf_6C_2N_4$	$Hf_6C_1N_5$	HfN
VEC	8.00	8.17	8.33	8.50	8.67	8.83	9.00
a_0 (Å)	4.651	4.629	4.612	4.590	4.568	4.552	4.533
ISF (J/m^2)	2.787	2.506	2.382	2.002	1.627	1.276	1.045
USF (J/m^2)	2.787	2.506	2.412	2.109	1.898	1.704	1.524
ISF/USF	1.000	1.000	0.988	0.949	0.857	0.749	0.686
$\tau^{RISS}_{\{111\}\langle112\rangle}$	25.0	24.5	26.4	25.0	24.6	24.8	23.5
$\tau^{RISS}_{\{111\}\langle110\rangle}$	34.2	32.1	33.4	32.1	32.8	32.6	30.0
$\tau^{RISS}_{\{110\}\langle110\rangle}$	24.5	21.6	18.8	21.8	27.5	27.3	26.2
$d^*_{0°}$	0.342	0.400	0.428	0.496	0.579	0.669	0.791
$d^*_{30°}$	0.410	0.480	0.513	0.595	0.695	0.804	0.949
$d^*_{45°}$	0.487	0.560	0.599	0.694	0.810	0.938	1.107
$d^*_{60°}$	0.547	0.640	0.684	0.793	0.926	1.071	1.265
$d^*_{90°}$	0.615	0.720	0.769	0.892	1.042	1.205	1.424

Note that the reported ISF and USF energies are respectively sampled from the local minimum and local maximum of the {111} ⟨112⟩ GSF energy curve, where applicable. These local extrema converge to form an inflection point with decreasing VEC, as can be seen in Fig. 8 (a). For GSF energy curves without defined local extrema in the region of interest, the inflection point is taken to be the location of both the ISF and the USF. For the analytically computed equilibrium separation distances, $d^*_\theta = d_\theta/a_0$ is the separation distance of the Shockley partials, scaled by the lattice constant, for a dislocation with some angle θ separating the line direction vector and burgers vector.

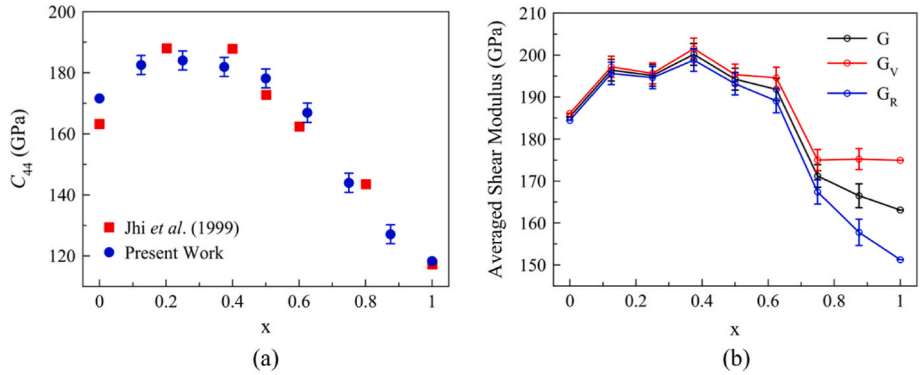

Fig. 4. (a) The variation of C44 with respect to HfN fraction *x*. The peak observed is consistent with the work of Jhi et al. [25] demonstrating a maximum around 0.25. (b) The Hill, Voigt, and Reuss shear moduli, also plotted with respect to HfN fraction *x*, illustrating a similar but delayed peak.

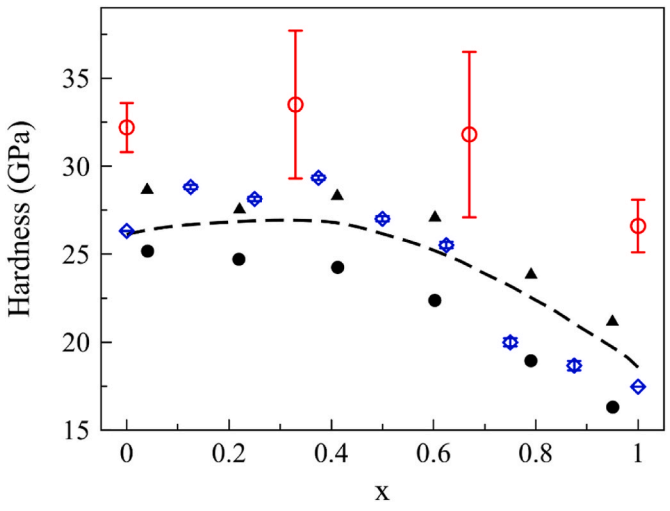

Fig. 5. Comparison of the theoretical Vickers hardness and experimental measurements of hardness plotted as a function of composition for $HfC_{1-x}N_x$ compounds. This includes the nanoindentation hardness reported here, the Vickers hardness trend claimed by Holleck [13], indicated by the dashed line, as well as the nanoindentation hardness (black triangle markers) and micro-indentation hardness (black circle markers) values obtained by Yang et al. [16].

without concrete evidence of a peak in hardness. The differences in experimental values can be attributed to the differences in indentation techniques (micro. vs. nano) and indentation loads/depths used in the measurements. The hardness trends are similar to those reported by Smith et al. in the HfC-TaC system, where theory predicted small enhancements near a VEC of 8.25 but similar experimental limitations could not definitively resolve this peak [26]. While collectively these results cannot rule out a hardness peak, they do confirm the point made above that any enhancement in elastic or hardness properties with composition is very small and cannot be exploited by composition engineering.

3.3. Dislocations and GSF curves

While the predictions of hardness from elastic constants is expedient, one should not expect the hardness to necessarily trend with elastic constants as strictly as precited by the equations used here. There are many reasons why this is true. First, the equations are fit for materials with large ranges in elastic constants and have large error for materials with similar elastic constants, like our hafnium carbonitrides. Second, hardness is a measurement that represents a materials resistance to local plastic flow, not elastic deformation. Thus, to understand how the hardness and the inelastic response of the hafnium carbonitrides could change with composition, it is critical to evaluate the behavior of dislocations, which are the fundamental carrier of plastic deformation in

TMCs/Ns subjected to indentation and low temperature creep. Fig. 6 is a representative SEM image of an indent taken from the $HfC_{0.67}N_{0.33}$ sample, where cracking as well as slip traces can be seen around the indent. These slip traces demonstrate that plasticity is active under the indents.

The as-computed GSF curves are shown in Fig. 7(a)–(c) for the ⟨112⟩{111}, ⟨110⟩{111}, and ⟨110⟩{110} slip systems. Fig. 7(a) shows that as the HfN concentration is increased, the ISF stabilizes and deepens, similar to the $Ta_xHf_{1-x}C$ system. All of the GSF curves decrease in magnitude as the HfN content is increased, making slip easier and thus likely enhancing plasticity. This matches the observations in previous experiments that seem to suggest that there is more localized plasticity in HfN than HfC and agrees with the experimental trends of hardness shown in Fig. 5.

As discussed by Yu et al., the unstable and intrinsic stacking faults as well as the rigid ideal shear strength are important for controlling on which plane the dislocations slip [30]. This is because the existence of an intrinsic stacking fault allows perfect dislocation on the {111} planes to split into Shockley partials separated by a stacking fault, e.g.:

$$\frac{1}{2}[10\bar{1}](111) \rightarrow \frac{1}{6}[2\bar{1}\bar{1}](111) + \frac{1}{6}[11\bar{2}](111)$$

The unstable stacking fault resists the motion of dislocations on the slip systems, and the rigid ideal shear strength also approximates the resistance to dislocation motion. Thus, they all relate to the intrinsic resistance to dislocation motion in these materials, which likely gives them strength.

The rigid ideal shear strength (RISS) is defined as:

$$\tau_P = \max\left[\frac{\partial\gamma}{\partial\delta}\right]$$

where $\gamma(\delta)$ is the misfit energy associated with a uniform disregistry δ across the shear plane. By sampling known disregistries, we can approximate $\gamma(\delta)$ with a GSF energy curve and thereby obtain estimates of $\partial\gamma/\partial\delta \approx \Delta\gamma/\Delta\delta$. The ISF and the unstable stacking-fault (USF) are easy to obtain for most compositions because they are the local minimum and maximum on the right half of the curve in Fig. 7(a). However, for very HfC-rich solutions, the ISF begins to disappear and eventually does. The same happens with the USF, because the USF and ISF collapse into an inflection point, which in this case is a monkey saddle [30,56]. Thus, we can approximate the ISF and USF as a single point where the curvature changes sign (or the slope reaches a minimum) in Fig. 7(a); we report these values in Table 3.

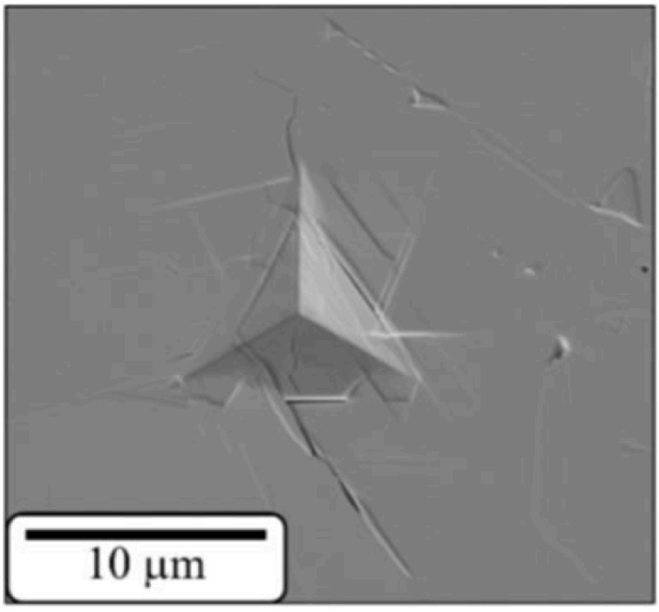

Fig. 6. SEM secondary electron image of an indent impression in the $HfC_{0.67}N_{0.33}$ sample. Note the apparent formation slip lines near the indent and the formation of linear microcracks along the rocksalt cleavage planes.

The RISS on the ⟨112⟩{111} system is relatively constant with x (VEC) as can be seen in Table 3 and in Fig. 7(a). This is because while the USF decreases with increasing x, the maximum slope occurs well before the USF and does not appear to change appreciably. The RISS on the ⟨110⟩{111} is similarly constant for the same reasons. The RISS for the ⟨110⟩{110} system actually does change, showing a dramatic decrease with intermediate concentrations. The reason for this is with initial increasing x, the peak drops and the slope goes down. However, past $x = 0.5$, the curves start to flatten out, which pushes the slopes up and causes the RISS to rise. If we use the RISS to determine the active slip systems, we would expect that HfC would slip on {110} while HfN would slip on {111} agreeing with experiments, with the transition occurring near the 50% composition when the ideal shear strength on the ⟨112⟩{111} and ⟨110⟩{110} cross. Thus, we can state based on the RISS that {111} slip is preferred for $x > 0.5$.

Another potential determining factor in the choice of slip planes is the existence of an ISF on the {111} planes which would stabilize the partial dislocations and the ability of the dislocations to split on the {111} planes. We can see that the ISF starts to stabilize for compositions $x > 0.33$. However, the splitting width of the partial dislocations is equally important because the wider the dislocations split, the easier they are to move. Therefore, we computed the splitting widths using the isotropic elasticity approximation:

$$d = \frac{G}{2\pi\gamma_{ISF}}\left(\frac{b_1^e b_2^e}{1-\nu} + b_1^s b_2^s\right)$$

where G is the shear modulus, γ_{ISF} is the ISF energy, ν is Poisson's ratio, and b_i^e and b_i^s are respectively the edge and screw components of the i^{th} partial dislocation. The calculated separation distances, scaled by the lattice constants of the various compositions, are shown in Table 3. For any character of perfect dislocation, the equilibrium separation can be seen to increase dramatically with increasing x (VEC). This suggests that dislocations on the {111} surfaces are increasingly mobile as VEC increases, making {111} slip available and eventually reducing the Peierls stress on {111} enough to change the slip system preference from ⟨110⟩{110} to ⟨110⟩{111}.

It should be noted that the depression of the ISF energy in the HfC-HfN system appears to be a much weaker effect than that observed in the HfC-TaC system by Smith et al. [26]. To demonstrate this, Fig. 8(a) shows the ISF plotted versus x (VEC) for our data and that of Smith et al. It is apparent that the rate of change of the ISF is stronger in the HfC-TaC system than the HfC-HfN system which allows the dislocations to split further apart in the HfC-TaC system as shown in Fig. 8(b). The rate of change of the ISF for the HfC-TaC system is 2.2 J/m^2/VEC as compared to the rate of change of 2.0 J/m^2/VEC per change in concentration (computed only for those value that have a stable ISF, 1.8 if inflection points are included). Given that Fig. 8(a) generally shows a linear variation ISF with composition (VEC) for each system, the difference largely lies in the ISF values of the end compounds. Thus, because HfN has a higher ISF value than TaC, adding HfN to HfC is less effective in reducing the ISF than adding TaC. Thus, the ISF transitions in these materials follow a simple rule of mixtures for the ISF energies. These results also point out that the VEC is not the only thing that controls the change in properties and that mixing metal atoms and non-metal atoms do not have the same effect. This is perhaps not surprising, but it means that if control over the properties of these materials is desired, the choice of which elements are mixed is important, not just the number of valence electrons.

The existence of an ISF in the group IVB nitrides — and the lack thereof in the group VB carbides — arises from subtle differences in bonding that exist between the two compounds despite their shared

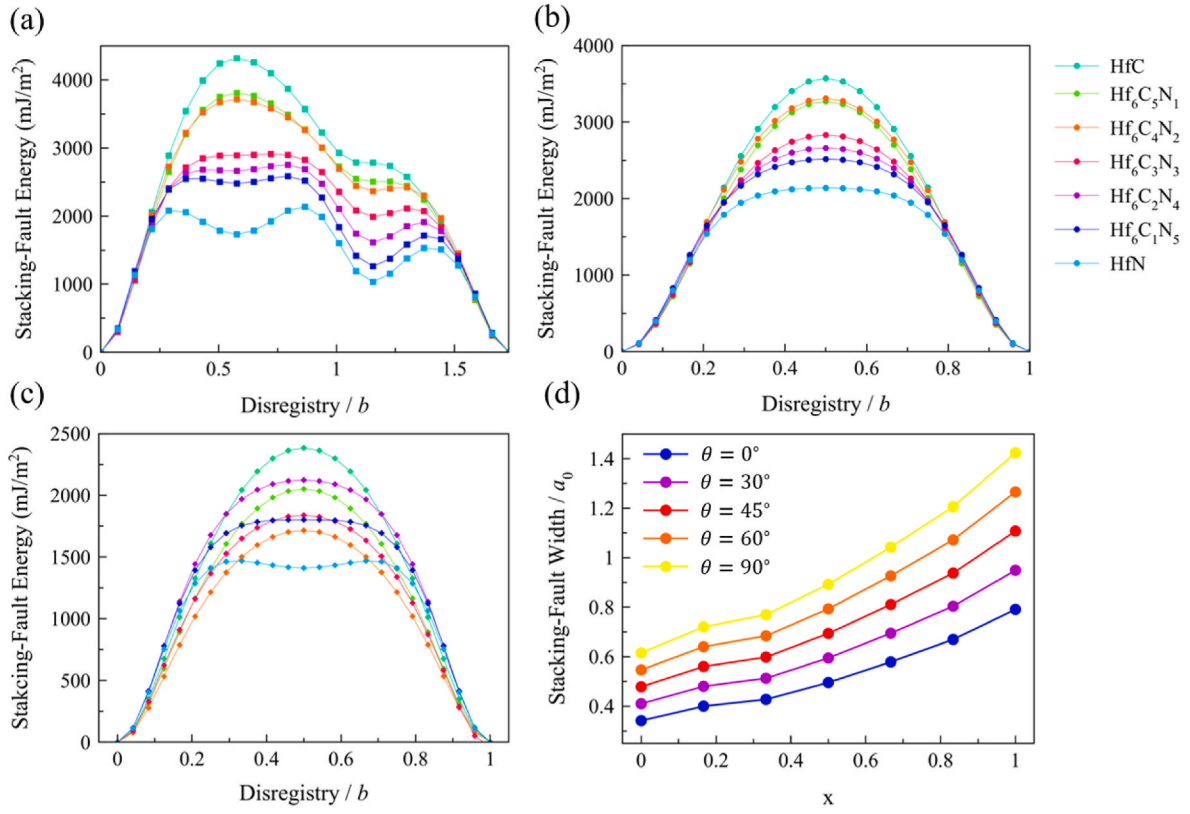

Fig. 7. The generalized stacking-fault energies in hafnium carbonitrides, for the (a) ⟨112⟩{111}, (b) ⟨110⟩{111}, and (c) ⟨110⟩{110} slip systems. The ISF becomes shallower as the HfN concentration is decreased (or VEC is decreased). (d) The computed Shockley partial dislocation separation distance as a function HfN concentration.

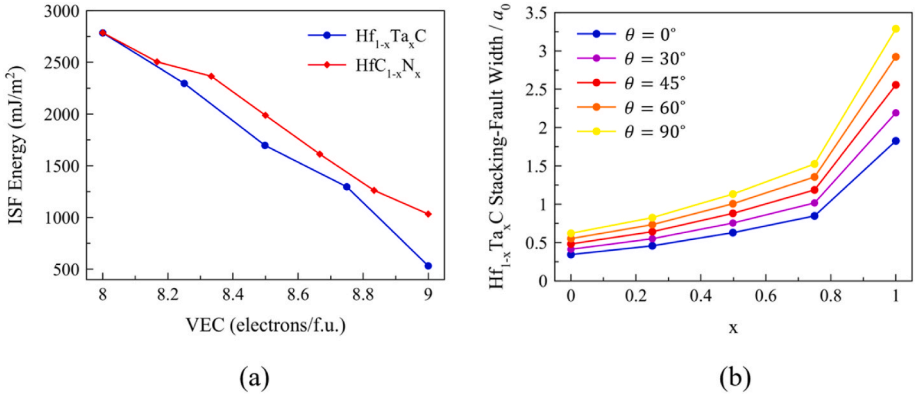

Fig. 8. (a) The ISF plotted as a function of x (VEC) for the HfC-TaC and HfC-HfN systems. The left two values for $HfC_{1-x}N_x$ are the inflection points. (b) The partial dislocation splitting widths as a function of x = Ta/(Hf + Ta), or the concentration of TaC in the HfC-TaC system. The different curves illustrate the behavior of dislocations with different edge and screw components.

crystal structure [28,30]. The extra electron in HfN presumably allows for more delocalized electrons and thus a more metallic bonding as argued by De Leon et al. [28]. To examine this in the HfC-HfN system, we computed the charge densities of the ideal compounds and those with stacking faults. The results, shown in Fig. 9, demonstrate that the electrons appear more delocalized in HfN than HfC. However, the iso-charge surfaces shown for HfN, Fig. 9(b), have more directional character than those observed for TaC (see Fig. 3 in Ref. [28]). Thus, it would appear that the bonds are moderately more directional in HfN than TaC, making the ISF less energetically favorable in HfN that TaC. Additionally, we included the computed electron localization function (ELF) [57,58] values in Fig. 10; these results suggest that additional bonding is present around the stacking-fault in HfN, Fig. 10(b), while there is no additional bonding visible in HfC, Fig. 10(a). This likely represents a stabilization of the B_h (WC) crystal structure with increasing VEC, since an ISF in the $B1$ structure is essentially a local phase transition to B_h. As VEC increases, then, the energy preference for the $B1$ structure over the B_h structure is diminished, and the ISF configuration becomes metastable.

We can postulate that the reason for TaC being the most metallic-like arises not only from more electrons than HfC, but a balance of the ions themselves as compared to HfN. Since the non-metal atoms are more electronegative, they should attract the electrons more strongly in the covalent bond. However, in the HfN system, the difference in

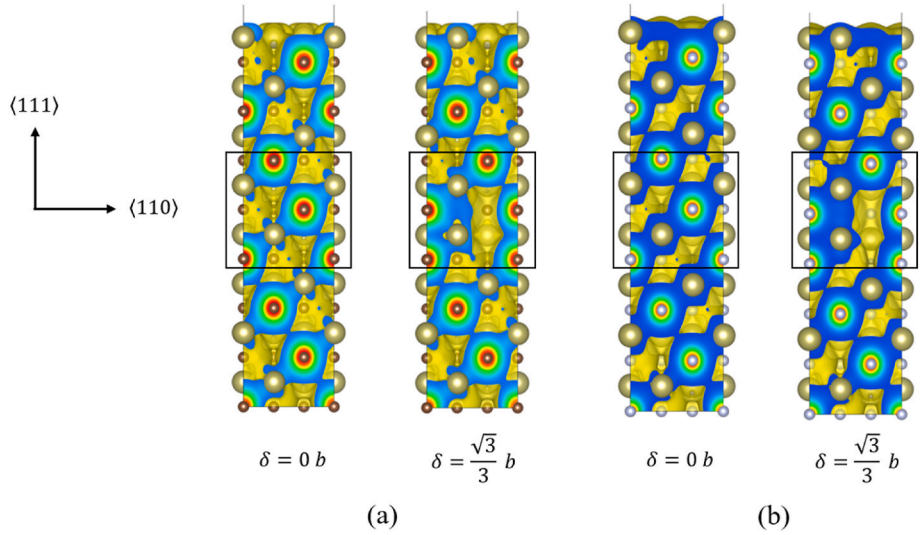

Fig. 9. Electron charge density in (a) HfC and (b) HfN. The additional electron present in HfN appears to facilitate charge delocalization, likely contributing to the stability of the ISF.

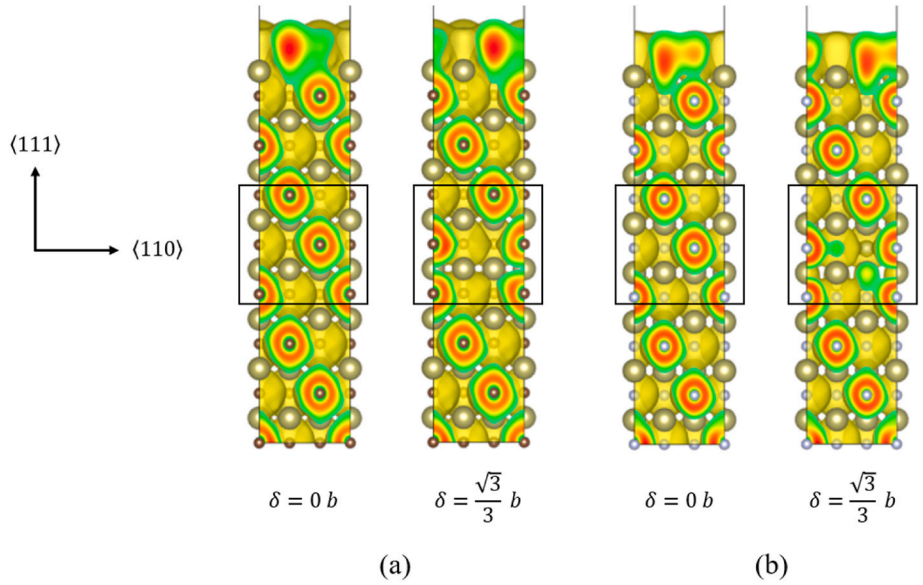

Fig. 10. Electron localization function (ELF) of (a) HfC and (b) HfN. An isosurface value of 0.30 is shown for all ELF figures. Note the regions of relatively high ELF between neighboring close-packed {111} planes of N atoms in HfN.

electronegativity is larger than the TaC system, so the bond is more directional in HfN than TaC. We note that these arguments are used to help explain the formation of intermetallics versus solid solutions in metals via the Hume-Rothery rules.

4. Conclusions

In this paper, we investigated how mixing, or alloying, a group IVB carbide with a group VB nitride affects the thermodynamics and mechanical properties of these materials. Specifically, this was done to investigate how changing the number of valence electrons via substation on the non-metal sublattice alters these properties and compare them with previous results of mixing group IVB carbides and VB carbides, where the same change in valence electrons occurred by missing the transition metals.

The evolutionary algorithm found a wide range of compounds on the convex hull, all of which are based on the rocksalt structure where the non-metal atoms ordered on their sublattice. The computed enthalpies of mixing suggest that HfC and HfN are completely miscible with a symmetric formation enthalpy curve and thus can be modeled as a subregular solution with a negative regular solution mixing parameter and that there is a very small energetic preference for ordering, suggesting that the solid solutions will usually be disordered.

The computed elastic constants and theoretical Vickers hardness do show a peak near the HfN composition of $x = 0.3$–0.4. However, the peak is modest—less than 10%—and experiments do not concretely show a peak, with the error of the measurements being larger than the variation with concentration near the maximum nominal value. These results are very similar to those observed in the HfC-TaC system with similar variations in VEC. Thus, the reported optimal VEC likely does not represent a promising avenue for hardness optimization in these materials.

The formation of solid solutions also changes the plastic response of these materials by altering dislocation behavior. The addition of HfN to

HfC lowers all GSF curves, generally decreasing the resistance to slip and making localized plasticity easier, which would likely compete with the enhanced stiffness due to small additions of nitrogen. The addition of HfC to HfN also starts to stabilize the ISF, similar to the addition of TaC to HfC. However, since HfN has a higher ISF than TaC, the amount of ISF reduction is lower per additional VEC. This has to do with electron sharing in the compounds of similar VEC, TaC as a lower electronegativity difference than HfN additions, making the bonds more metallic like in TaC than HfN. Thus, the addition of TaC is likely to make localized plasticity easier in HfC than HfN, but not substantially more. This indicates that, while VEC has a pronounced effect, electronegativity differences are important for understanding how metal and nonmetal mixing influences the mechanical properties of the *B*1-structured carbonitrides.

Declaration of competing interest

The authors declare that they have no known competing financial interests or personal relationships that could have appeared to influence the work reported in this paper.

Acknowledgements

This material is based upon work supported by the National Science Foundation under Grant No. NSF-DMR-2026766 (BRW and CRW) and NSF-DMR-2026760 (JL and GBT). This work utilized the RMACC Summit supercomputer, which is supported by the National Science Foundation (awards ACI-1532235 and ACI-1532236), the University of Colorado Boulder and Colorado State University. The RMACC Summit supercomputer is a joint effort of the University of Colorado Boulder and Colorado State University.

Appendix A. Supplementary data

Supplementary data to this article can be found online at https://doi.org/10.1016/j.oceram.2023.100356.

References

[1] E. Wuchina, E. Opila, M. Opeka, W. Fahrenholtz, I. Talmy, UHTCs: ultra-high temperature ceramic materials for extreme environment applications, Electrochem. Soc. Interface 16 (2007) 30–36.
[2] W.S. Williams, Cubic Carbides: solid-state physics explores materials having ionic structure, metallic conductivity, and covalent hardness, Science 152 (1966) 34–42, https://doi.org/10.1126/science.152.3718.34.
[3] L. Toth, Transition Metal Carbides and Nitrides, Academic Press, New York, 1971.
[4] W. Fahrenholtz (Ed.), Ultra-high Temperature Ceramics: Materials for Extreme Environment Applications, The America Ceramic Society/Wiley, Hoboken, New Jersey, 2014.
[5] E.P. Simonenko, D.V. Sevast'yanov, N.P. Simonenko, V.G. Sevast'yanov, N. T. Kuznetsov, Promising ultra-high-temperature ceramic materials for aerospace applications, Russ. J. Inorg. Chem. 58 (2013) 1669–1693, https://doi.org/10.1134/S0036023613140039.
[6] A.T. Santhanam, Application of transition metal carbides and nitrides in industrial tools, in: S.T. Oyama (Ed.), The Chemistry of Transition Metal Carbides and Nitrides, Springer Netherlands, Dordrecht, 1996, pp. 28–52, https://doi.org/10.1007/978-94-009-1565-7_2.
[7] H.O. Pierson, Handbook of Refractory Carbides and Nitrides: Properties, Characteristics, Processing, and Applications, Noyes Publications, Park Ridge, N.J, 1996.
[8] O. Cedillos-Barraza, D. Manara, K. Boboridis, T. Watkins, S. Grasso, D. D. Jayaseelan, R.J.M. Konings, M.J. Reece, W.E. Lee, Investigating the highest melting temperature materials: a laser melting study of the TaC-HfC system, Sci. Rep. 6 (2016), 37962, https://doi.org/10.1038/srep37962.
[9] C. Agte, H. Alterthum, Systems of high-melting carbides: contributions to the problem carbon fusion, Tech. Phys. 11 (1930) 182–191.
[10] R.A. Andrievskii, N.S. Strel'nikova, N.I. Poltoratskii, E.D. Kharkhardin, V. S. Smirnov, Melting point in systems ZrC-HfC, TaC-ZrC, TaC-HfC, Poroshkovaya Metall. 1 (1967) 85–88.
[11] D.L. Deadmore, Vaporization of tantalum carbide-hafnium carbide solid solutions, J. Am. Ceram. Soc. 48 (1965) 357–359, https://doi.org/10.1111/j.1151-2916.1965.tb14760.x.
[12] Q.-J. Hong, A. van de Walle, Prediction of the material with highest known melting point from *ab initio* molecular dynamics calculations, Phys. Rev. B 92 (2015), 020104, https://doi.org/10.1103/PhysRevB.92.020104 (R).
[13] H. Holleck, Material selection for hard coatings, J. Vac. Sci. Technol. A: Vacuum, Surfaces, and Films 4 (1986) 2661–2669, https://doi.org/10.1116/1.573700.
[14] K. Balasubramanian, S.V. Khare, D. Gall, Valence electron concentration as an indicator for mechanical properties in rocksalt structure nitrides, carbides and carbonitrides, Acta Mater. 152 (2018) 175–185, https://doi.org/10.1016/j.actamat.2018.04.033.
[15] S.-H. Jhi, J. Ihm, Electronic structure and structural stability of TiC x N 1 − x alloys, Phys. Rev. B 56 (1997) 13826–13829, https://doi.org/10.1103/PhysRevB.56.13826.
[16] Q. Yang, W. Lengauer, T. Koch, M. Scheerer, I. Smid, Hardness and elastic properties of Ti(CxN1−x), Zr(CxN1−x) and Hf(CxN1−x), J. Alloys Compd. 309 (2000) L5–L9, https://doi.org/10.1016/S0925-8388(00)01057-4.
[17] V.S. Buinevich, A.A. Nepapushev, D.O. Moskovskikh, G.V. Trusov, K.V. Kuskov, S. G. Vadchenko, A.S. Rogachev, A.S. Mukasyan, Fabrication of ultra-high-temperature nonstoichiometric hafnium carbonitride via combustion synthesis and spark plasma sintering, Ceram. Int. 46 (2020) 16068–16073, https://doi.org/10.1016/j.ceramint.2020.03.158.
[18] P. Sarker, T. Harrington, C. Toher, C. Oses, M. Samiee, J.-P. Maria, D.W. Brenner, K.S. Vecchio, S. Curtarolo, High-entropy high-hardness metal carbides discovered by entropy descriptors, Nat. Commun. 9 (2018) 4980, https://doi.org/10.1038/s41467-018-07160-7.
[19] Y. Wang, Processing and properties of high entropy carbides, Adv. Appl. Ceram. 121 (2022) 57–78, https://doi.org/10.1080/17436753.2021.2014277.
[20] O.F. Dippo, N. Mesgarzadeh, T.J. Harrington, G.D. Schrader, K.S. Vecchio, Bulk high-entropy nitrides and carbonitrides, Sci. Rep. 10 (2020), 21288, https://doi.org/10.1038/s41598-020-78175-8.
[21] H. Xiang, Y. Xing, F. Dai, H. Wang, L. Su, L. Miao, G. Zhang, Y. Wang, X. Qi, L. Yao, H. Wang, B. Zhao, J. Li, Y. Zhou, High-entropy ceramics: present status, challenges, and a look forward, J Adv Ceram 10 (2021) 385–441, https://doi.org/10.1007/s40145-021-0477-y.
[22] R.-Z. Zhang, M.J. Reece, Review of high entropy ceramics: design, synthesis, structure and properties, J. Mater. Chem. A. 7 (2019) 22148–22162, https://doi.org/10.1039/C9TA05698J.
[23] D.G. Sangiovanni, W. Mellor, T. Harrington, K. Kaufmann, K. Vecchio, Enhancing plasticity in high-entropy refractory ceramics via tailoring valence electron concentration, Mater. Des. 209 (2021), 109932, https://doi.org/10.1016/j.matdes.2021.109932.
[24] D.G. Sangiovanni, V. Chirita, L. Hultman, Electronic mechanism for toughness enhancement in Ti x M 1 − x N (M = Mo and W), Phys. Rev. B 81 (2010), 104107, https://doi.org/10.1103/PhysRevB.81.104107.
[25] S.-H. Jhi, J. Ihm, S.G. Louie, M.L. Cohen, Electronic mechanism of hardness enhancement in transition-metal carbonitrides, Nature 399 (1999) 132–134, https://doi.org/10.1038/20148.
[26] C.J. Smith, X.-X. Yu, Q. Guo, C.R. Weinberger, G.B. Thompson, Phase, hardness, and deformation slip behavior in mixed HfxTa1-xC, Acta Mater. 145 (2018) 142–153, https://doi.org/10.1016/j.actamat.2017.11.038.
[27] I.M. Vinitskii, Relation between the properties of monocarbides of groups IV?V transition metals and their carbon content, Sov. Powder Metall. Met. Ceram. 11 (1972) 488–493, https://doi.org/10.1007/BF00797927.
[28] N. De Leon, X. Yu, H. Yu, C.R. Weinberger, G.B. Thompson, Bonding effects on the slip differences in the B 1 monocarbides, Phys. Rev. Lett. 114 (2015), 165502, https://doi.org/10.1103/PhysRevLett.114.165502.
[29] K. Vinson, X.-X. Yu, N. De Leon, C.R. Weinberger, G.B. Thompson, Plasticity mechanisms in HfN at elevated and room temperature, Sci. Rep. 6 (2016), 34571, https://doi.org/10.1038/srep34571.
[30] H. Yu, M. Bahadori, G.B. Thompson, C.R. Weinberger, Understanding dislocation slip in stoichiometric rocksalt transition metal carbides and nitrides, J. Mater. Sci. 52 (2017) 6235–6248, https://doi.org/10.1007/s10853-017-0857-4.
[31] A.R. Oganov, C.W. Glass, Crystal structure prediction using *ab initio* evolutionary techniques: principles and applications, J. Chem. Phys. 124 (2006), 244704, https://doi.org/10.1063/1.2210932.
[32] C.W. Glass, A.R. Oganov, N. Hansen, USPEX—evolutionary crystal structure prediction, Comput. Phys. Commun. 175 (2006) 713–720, https://doi.org/10.1016/j.cpc.2006.07.020.
[33] A.O. Lyakhov, A.R. Oganov, H.T. Stokes, Q. Zhu, New developments in evolutionary structure prediction algorithm USPEX, Comput. Phys. Commun. 184 (2013) 1172–1182, https://doi.org/10.1016/j.cpc.2012.12.009.
[34] G. Kresse, J. Furthmüller, Efficient iterative schemes for *ab initio* total-energy calculations using a plane-wave basis set, Phys. Rev. B 54 (1996) 11169–11186, https://doi.org/10.1103/PhysRevB.54.11169.
[35] G. Kresse, J. Hafner, *Ab initio* molecular dynamics for liquid metals, Phys. Rev. B 47 (1993) 558–561, https://doi.org/10.1103/PhysRevB.47.558.
[36] G. Kresse, D. Joubert, From ultrasoft pseudopotentials to the projector augmented-wave method, Phys. Rev. B 59 (1999) 1758–1775, https://doi.org/10.1103/PhysRevB.59.1758.
[37] C.R. Weinberger, X.-X. Yu, H. Yu, G.B. Thompson, Ab initio investigations of the phase stability in group IVB and VB transition metal nitrides, Comput. Mater. Sci. 138 (2017) 333–345, https://doi.org/10.1016/j.commatsci.2017.07.005.
[38] X.-X. Yu, C.R. Weinberger, G.B. Thompson, Ab initio investigations of the phase stability in group IVB and VB transition metal carbides, Comput. Mater. Sci. 112 (2016) 318–326, https://doi.org/10.1016/j.commatsci.2015.10.038.
[39] Q. Zeng, J. Peng, A.R. Oganov, Q. Zhu, C. Xie, X. Zhang, D. Dong, L. Zhang, L. Cheng, Prediction of stable hafnium carbides: stoichiometries, mechanical

properties, and electronic structure, Phys. Rev. B 88 (2013), https://doi.org/10.1103/PhysRevB.88.214107.
[40] X.-X. Yu, C.R. Weinberger, G.B. Thompson, Ab initio investigations of the phase stability in tantalum carbides, Acta Mater. 80 (2014) 341–349, https://doi.org/10.1016/j.actamat.2014.07.070.
[41] S. Yu, Q. Zeng, A.R. Oganov, G. Frapper, L. Zhang, Phase stability, chemical bonding and mechanical properties of titanium nitrides: a first-principles study, Phys. Chem. Chem. Phys. 17 (2015) 11763–11769, https://doi.org/10.1039/C5CP00156K.
[42] A.R. Oganov (Ed.), Modern Methods of Crystal Structure Prediction, first ed., Wiley, 2010 https://doi.org/10.1002/9783527632831.
[43] A. van de Walle, M. Asta, G. Ceder, The alloy theoretic automated toolkit: a user guide, Calphad 26 (2002) 539–553, https://doi.org/10.1016/S0364-5916(02)80006-2.
[44] P.E. Blöchl, Projector augmented-wave method, Phys. Rev. B 50 (1994) 17953–17979, https://doi.org/10.1103/PhysRevB.50.17953.
[45] J.P. Perdew, K. Burke, M. Ernzerhof, Generalized gradient approximation made simple, Phys. Rev. Lett. 77 (1996) 3865–3868, https://doi.org/10.1103/PhysRevLett.77.3865.
[46] H.J. Monkhorst, J.D. Pack, Special points for Brillouin-zone integrations, Phys. Rev. B 13 (1976) 5188–5192, https://doi.org/10.1103/PhysRevB.13.5188.
[47] F. Vogel, S. Ngai, C.J. Smith, R. Holler, C.R. Weinberger, N. Wanderka, G. B. Thompson, Carbide and nitride phase characterization in a transition metal carbo-nitride using x-ray spectroscopy and atom probe tomography, Micron 122 (2019) 32–40, https://doi.org/10.1016/j.micron.2019.04.005.
[48] W.C. Oliver, G.M. Pharr, Measurement of hardness and elastic modulus by instrumented indentation: advances in understanding and refinements to methodology, J. Mater. Res. 19 (2004) 3–20, https://doi.org/10.1557/jmr.2004.19.1.3.
[49] A. Zunger, S.-H. Wei, L.G. Ferreira, J.E. Bernard, Special quasirandom structures, Phys. Rev. Lett. 65 (1990) 353–356, https://doi.org/10.1103/PhysRevLett.65.353.
[50] A. Markström, D. Andersson, K. Frisk, Combined ab-initio and experimental assessment of mixed carbides, Calphad 32 (2008) 615–623, https://doi.org/10.1016/j.calphad.2008.07.014.
[51] X. Tang, G.B. Thompson, K. Ma, C.R. Weinberger, The role of entropy and enthalpy in high entropy carbides, Comput. Mater. Sci. 210 (2022), 111474, https://doi.org/10.1016/j.commatsci.2022.111474.
[52] V.I. Ivashchenko, P.E.A. Turchi, N.R. Medukh, V.I. Shevchenko, L. Gorb, J. Leszczynski, A first-principles study of the stability and mechanical properties of ternary transition metal carbide alloys, J. Appl. Phys. 125 (2019), 235101, https://doi.org/10.1063/1.5096646.
[53] W. Cai, W.D. Nix, Imperfections in Crystalline Solids, first ed., Cambridge University Press, 2016 https://doi.org/10.1017/CBO9781316389508.
[54] R.E. Newnham, Properties of Materials: Anisotropy, Symmetry, Structure, Oxford University Press, Oxford ; New York, 2005.
[55] X.-Q. Chen, H. Niu, D. Li, Y. Li, Modeling hardness of polycrystalline materials and bulk metallic glasses, Intermetallics 19 (2011) 1275–1281, https://doi.org/10.1016/j.intermet.2011.03.026.
[56] Scott Peckman, Monkey, starfish and Octopus saddles, Proceedings of Geomorphometry (2011) 31–34.
[57] B. Silvi, A. Savin, Classification of chemical bonds based on topological analysis of electron localization functions, Nature 371 (1994) 683–686, https://doi.org/10.1038/371683a0.
[58] K. Koumpouras, J.A. Larsson, Distinguishing between chemical bonding and physical binding using electron localization function (ELF), J. Phys. Condens. Matter 32 (2020), 315502, https://doi.org/10.1088/1361-648X/ab7fd8.